

High Dynamic Range Imaging Concept-Based Signal Enhancement Method Reduced the Optical Coherence Tomography Measurement Variability

Hiroshi Ishikawa,¹⁻³ Chieh-Li Chen,¹⁻³ Gadi Wollstein,¹ Jonathan L. Grimm,¹ Yun Ling,^{1,4} Richard A. Bilonick,^{1,4} Ian A. Sigal,^{1,2} Larry Kagemann,^{1,2} and Joel S. Schuman^{1,2}

PURPOSE. To develop and test a novel signal enhancement method for optical coherence tomography (OCT) images based on the high dynamic range (HDR) imaging concept.

METHODS. Three virtual channels, which represent low, medium, and high signal components, were produced for each OCT signal dataset. The dynamic range of each signal component was normalized to the full gray scale range. Finally, the three components were recombined into one image using various weights. Fourteen eyes of 14 healthy volunteers were scanned multiple times using time-domain (TD)-OCT before and while preventing blinking in order to produce a wide variety of signal strength (SS) images on the same eye scanned on the same day. For each eye, a pair of scans with the highest and lowest SS with successful retinal nerve fiber layer (RNFL) segmentation was selected to test the signal enhancement effect. In addition, spectral-domain (SD)-OCT images with poor signal qualities were also processed.

RESULTS. Mean SS of good and poor quality scans were 9.0 ± 1.1 and 4.4 ± 0.9 , respectively. TD-OCT RNFL thickness showed significant differences between good and poor quality scans on the same eye (mean difference $11.9 \pm 6.0 \mu\text{m}$, $P < 0.0001$, paired *t*-test), while there was no significant difference after signal enhancement ($1.7 \pm 6.2 \mu\text{m}$, $P = 0.33$). However, HDR had weaker RNFL compensation effect on images with SS less than or equal to 4, while it maintained good compensation

effect on images with SS greater than 4. Successful signal enhancement was also confirmed subjectively on SD-OCT images.

CONCLUSION. The HDR imaging successfully restored OCT signal and image quality and reduced RNFL thickness differences due to variable signal level to the level within the expected measurement variability. This technique can be applied to both TD- and SD-OCT images. (*Invest Ophthalmol Vis Sci.* 2013;54:836-841) DOI:10.1167/iovs.12-10990

Optical coherence tomography (OCT) is a noninvasive and noncontact imaging technique. It generates volumetric, in vivo, cross-sectional images with microscopic resolution of the ocular tissues in a real time fashion by measuring the interference of the reflected signal from the reference mirror and the back of the eye.¹⁻³ OCT has become an indispensable tool in ophthalmology clinical routines for both qualitative and quantitative assessment of ocular tissues.⁴⁻⁷

It is well known, however, that signal quality variability affects our ability to interpret and analyze OCT images.^{8,9} Retinal nerve fiber layer (RNFL) thickness measurements showed a significant positive correlation with the signal level.⁸⁻¹⁰ Qualitative evaluation of OCT images is also markedly influenced from the signal level.¹¹⁻¹³ There have been several attempts to enhance OCT images with relatively low signal level,¹⁴⁻¹⁶ but to our knowledge there is none that proved to be effective to address OCT measurement variability within the same image due to variable signal level.

High dynamic range (HDR) imaging technology, which has a long history in photography, expands the image contrast dynamic range by combining multiple images with different exposure settings.¹⁷⁻²² However, with OCT scanning, acquiring multiple scans with different exposure settings, is not feasible as the exposure level cannot be controlled mechanically/optically. We hypothesize that the HDR concept can be applied to enhance OCT images and achieve greater dynamic range in both weak and strong signal areas without the need of multiple scans, and that the HDR imaging technique can be used to compensate signal level differences in both qualitative as well as quantitative OCT image assessment.

Hence, the purpose of this study was to develop and test a novel signal enhancement method for OCT images based on the HDR imaging concept without the need of multiple scans in different exposures. For its validation, a set of OCT images obtained under varying corneal dryness conditions causing fluctuating image quality was processed to see the effect on RNFL thickness measurements between good and poor signal strength images scanned on the same eye.

From the ¹University of Pittsburgh Medical Center Eye Center, Eye and Ear Institute, Ophthalmology and Visual Science Research Center, Department of Ophthalmology, University of Pittsburgh School of Medicine, Pittsburgh, Pennsylvania; and the ²Department of Bioengineering, Swanson School of Engineering, and the ⁴Department of Biostatistics, Graduate School of Public Health, University of Pittsburgh, Pittsburgh, Pennsylvania.

³These authors contributed equally to the work presented here and should therefore be regarded as equivalent authors.

Presented in part at the annual meeting of the Association for Research in Vision and Ophthalmology, Fort Lauderdale, Florida, May 2012.

Supported by grants in part by National Institutes of Health (R01-EY013178, R01-EY011289, P30-EY008098), The Eye and Ear Foundation, and unrestricted grants from Research to Prevent Blindness.

Submitted for publication September 19, 2012; revised December 11, 2012; accepted December 15, 2012.

Disclosure: **H. Ishikawa**, None; **C.-L. Chen**, None; **G. Wollstein**, Allergan (C); **J.L. Grimm**, None; **Y. Ling**, None; **R.A. Bilonick**, None; **I.A. Sigal**, None; **L. Kagemann**, None; **J.S. Schuman**, P

Corresponding author: Gadi Wollstein, UPMC Eye Center, Eye and Ear Institute, 203 Lothrop Street, Pittsburgh, PA 15213; wollsteing@upmc.edu.

METHODS

HDR Imaging

The HDR imaging includes two major stages:

Step 1: Three virtual OCT signal channels processing

For each B-scan image, four histogram parameters, minimum, maximum, noise level, and saturation level, were calculated based on a previous study,¹¹ where minimum and maximum are the lowest and highest pixel values of the entire B-scan image, respectively, noise level was defined as the 66th percentile of the pixel value, and saturation level was defined as the 99th percentile of the pixel value of the entire B-scan. For each frame, the original OCT signal dataset was divided into three datasets, creating three virtual channels: low, medium, and high signal channels. The low signal channel, I_{Low} , consisted of pixel values between minimum and low offset values, the high signal channel, I_{Highb} , consisted of pixel values between high offset and saturation level values, and the medium signal, I_{Mid} , consisted of pixel values between low offset and high offset values, where low offset and high offset are defined as Equation 1:

$$\text{Low Offset} = \text{Noise} + 0.23 \times (\text{Saturation} - \text{Noise}),$$

$$\text{High Offset} = \text{Saturation} - 0.067 \times (\text{Saturation} - \text{Noise}) \quad (1)$$

Each dataset was then processed to maximize the signal dynamic range by linearly rescaling pixel values between lowest and highest values in each dataset to the full 8-bit gray scale range (0 to 255) in each B-scan. The intensity value outside of the defined cutoff values (lower or higher) was forced to be either 0 or 255.

Step 2: High dynamic range signal composition

After processing each virtual signal channel, signals from all three channels were combined to generate the final HDR dataset by calculating weighted mean values of the three channels, as shown in Equation 2,

$$I_{HDR}(x, z) = \frac{1}{c_L + c_M + c_H} (c_L \times I_{Low}(x, z) + c_M \times I_{Mid}(x, z) + c_H \times I_{Highb}(x, z)) \quad (2)$$

where I_{Low} , I_{Mid} , I_{Highb} , and I_{HDR} stand for low, mid, and high signal channels and the output image after HDR imaging, respectively; $I(x, z)$ indicates the pixel value at position (x, z) in the processed B-scan, (i.e., x^{th} A-scan and z^{th} pixel in the axial direction; and c_L , c_M , and c_H are the weighted coefficients). The coefficients used for calculating the weighted mean are adjusted as a function of the signal strength of the original image so that the image quality can be enhanced for OCT images with poor signal strength, while preventing the images with good signal strength from becoming saturated. In general, the coefficients were centered around 3.0 for c_L , 2.0 for c_M , and 1.0 for c_H .

HDR Imaging Performance Testing

Subjects included in this study were recruited at the University of Pittsburgh Medical Center Eye Center. The University of Pittsburgh review board and ethics committee approval were obtained for the study and informed consents were obtained from all subjects. This study followed the tenets of the Declaration of Helsinki and was conducted in compliance with the Health Insurance Portability and Accountability Act.

Two experiments were designed to test the performance of the proposed HDR imaging on OCT images. In the first experiment, we tested the signal level compensation ability of the HDR imaging using our previous time-domain (TD)-OCT data, which had a wide range of signal strengths (SSs).⁸ In the second experiment, we moved forward onto spectral-domain (SD)-OCT data to assess the image appearance after HDR imaging and to show that the HDR imaging also works on SD-OCT data.

Experiment 1: Effects of Signal Level Compensation on Quantitative Analysis

This experiment was designed to test the effects of our HDR imaging on signal level compensation for quantitative analysis. To test the compensation ability, the variability in RNFL thickness measurements on images scanned with various signal levels of the same eye was measured.

Subjects and Image Acquisition. Ocular images obtained in a previous study were used in this experiment.⁸ Seventeen eyes of 17 healthy volunteers were scanned with the TD-OCT Fast RNFL scanning protocol (Stratus OCT; Carl Zeiss Meditec, Dublin, CA). The TD-OCT Fast RNFL scanning protocol generates three consecutive, circum-papillary RNFL images at a scanning radius of 3.4 mm centered on the optic nerve head. The upper eyelid of each subject was taped to the forehead on the selected, anesthetized eye to prevent blinking so that a wide variety of signal level images on the same eye can be acquired. OCT image was acquired every 20 seconds for a total of eight series of images per eye. After the drying scans, the tape was removed and the subject was allowed to blink normally, then three more scans were acquired at 1, 2, and 4 minutes after removing the tape. In this way, we would have the ultimate reference scans (the scans with highest SS) and the deteriorated scans all acquired from the same eye and same session removing all/most other potential confounders. All the raw image data were exported to a standalone computer (MacBook Pro; Apple, Cupertino, CA) for further HDR imaging.

Both the original OCT data and the HDR imaging OCT data were then processed with our custom segmentation algorithm to measure RNFL thickness.²³ For the original OCT data, RNFL thickness was also measured with the original machine built-in segmentation algorithm. Segmentation results were subjectively evaluated for accuracy of the automated RNFL border detection. Scans were excluded if the images demonstrated one or both of the following: (1) apparent inaccurate border detection for more than consecutive 15% or additive 20% of the total image, or (2) borders of the RNFL collapsed, meaning that the RNFL thickness was recoded as a string of zeros for at least 10 consecutive points. The mean of at least two qualified scans (from the three scans acquired in each series) for each time point was used for the analysis.

Finally, a pair of scans, which were the scans with the highest and lowest signal level but without RNFL segmentation failures, was selected for each eye to compare the HDR imaging effect.

Experiment 2: Effects of Image Quality Enhancement

This experiment was designed to test the effects of our HDR imaging technology on OCT image enhancement. To test the image enhancement ability, several OCT images with a poor signal level were processed with our HDR imaging, and the visibility of the intraretinal layers before and after HDR imaging was subjectively assessed by an observer (CLC). In addition, objective image quality assessment was further applied on a separate dataset with 270 SD-OCT images showing good signal levels to test the effects of our HDR imaging technology on the normal, clinically acceptable images.

Image Enhancement Ability Assessment

Subjects and Image Acquisition. Fifteen eyes of 15 subjects (eight healthy and seven glaucoma) were enrolled. Poor quality images obtained with two SD-OCT devices were assembled for this study (Cirrus HD-OCT; Carl Zeiss Meditec, or RTVue; Optovue, Fremont, CA). Qualified OCT images had signal levels below the manufacturer recommended cutoff: SS less than 7 for Cirrus and SS index less than 40 for RTVue.

Visibility of intraretinal layers was subjectively assessed before and after HDR imaging by presenting both images (before and after HDR) in

a random order. The observer judged if there was a notable difference in visibility on each pair. In addition, a custom retinal segmentation algorithm (the one used in Experiment 1) was also performed on both original and HDR processed OCT images to test the possible improvement on segmentation performance after HDR imaging.

Objective Image Quality Assessment. One hundred thirty-six eyes from 95 subjects (32 healthy, 22 glaucoma suspect, and 41 glaucoma subjects) were enrolled. High quality images, which were eligible for clinical diagnoses and image analyses, obtained with two SD-OCT devices were assembled for this study (Cirrus HD-OCT and RTVue). Qualified OCT images had signal levels above the manufacturer recommended cutoff: SS higher than 6 for Cirrus and signal strength index higher than 40 for RTVue.

Signal-to-noise ratio (SNR) and contrast-to-noise ratio (CNR) were used to objectively evaluate the performance of the proposed HDR imaging technology of 270 SD-OCT images. SNR measures the signal level of a desired signal to the signal level of the noise model and CNR measures the difference between an area of image feature and an area of background noise. The definitions for these image quality metrics for a single frame are described in the literature as follows²⁴⁻²⁶:

$$\text{SNR} = 10 \log \left(\frac{\max(I^2)}{\sigma_n^2} \right),$$

$$\text{CNR} = 10 \log \left(\frac{\mu_f - \mu_n}{\sqrt{\sigma_f^2 + \sigma_n^2}} \right) \quad (3)$$

In the expression for SNR, I represents the logged value from the OCT machine output, and σ_n^2 stands for the variance of the background noise region in the logged value. In the CNR formula, μ_f and μ_n indicate the mean value of the selected regions of interest and of the same background noise region as in SNR, while σ_f^2 and σ_n^2 stand for the variance of the selected regions of interest and of the same background noise region as in SNR. As HDR processed images are clipped at the saturation level (99th percentile), SNR and CNR calculations were done on original images after the same clipping was applied. This also prevents erroneous measurements due to a few exceptionally high intensity outlier pixels.

To measure the SNR and CNR for the entire cube data, we modified Equation 3 to:

$$\text{SNR} = 10 \log \left(\frac{\sum_{m=1}^M \left(\frac{\max(I^2)}{\sigma_n^2} \right)_m}{M} \right),$$

$$\text{CNR} = 10 \log \left(\frac{\sum_{m=1}^M \left(\frac{\mu_f - \mu_n}{\sqrt{\sigma_f^2 + \sigma_n^2}} \right)_m^2}{M} \right) \quad (4)$$

In Equation 4, intermediate SNR and CNR for each frame were calculated and accumulated and the final SNR and CNR values were assessed using the arithmetic average of the intermediate parameters, where M stands for the number of frames in one cube data. For SNR and CNR calculation, signals located in a rectangular region at the bottom of each B-scan, with the same width as the B-scan and height as 3% of the axial pixel number, were considered as the noise signal, so that we had the minimal chance to include true retinal signal into the noise signal model, which was used to calculate μ_n and σ_n . An additional four regions were automatically located in the RNFL, ganglion cell and inner plexiform layer (GC-IPL), inner nuclear and outer plexiform layer (IN-OPL), and RPE based on the position of the inner limiting membrane (ILM), outer RNFL border, and RPE from the segmentation results using our custom segmentation software.²³ The CNR values were averaged over the four regions of interest, while the SNR used the entire image as the region of interest.

Statistical Analysis

The relationship between RNFL thickness measurements and SS of OCT images was measured using linear regression models for each of the following RNFL thickness segmentation algorithms: the original device built-in algorithm (Device) and our custom algorithm with or without HDR imaging (Custom or HDR, respectively). Paired t -tests were used to analyze the image quality metrics (SNR and CNR) improvement between the original and HDR processed images. P values less than 0.05 were considered statistically significant.

RESULTS

Experiment 1: Effects of Signal Level Compensation on Quantitative Analysis

In total, 951 images were collected, and 109 (11.5%) of them (mean SS 2.7 ± 1.1) were excluded from the study due to the segmentation failure. The overall mean SS of the original TD-OCT images was 6.6 ± 2.4 , ranging from 0 to 10 (the full range of the SS for the TD-OCT device). Mean SS of good and poor quality scans were 9.0 ± 1.1 and 4.4 ± 0.9 , respectively. Prior to signal level enhancement, the RNFL thickness showed significant differences between good and poor quality scans on the same eye (mean RNFL difference $11.9 \pm 1.6 \mu\text{m}$, $P < 0.0001$, paired t -test). This difference became substantially smaller and nonsignificant after HDR imaging, where the mean difference was $1.7 \pm 1.7 \mu\text{m}$ ($P = 0.33$). This result fits well within the expected test-retest measurement variability, which is $10 \mu\text{m}$ for TD-OCT images with good signal level.²⁷

The RNFL thickness showed two separate linear relationships with SS above or below 4 for all algorithms (Device, Custom, and HDR; Fig. 1). In the range of SS greater than 4, the HDR algorithm showed a smaller slope ($-0.01 \mu\text{m}$) in the relationship between RNFL thickness and SS compared with other algorithms ($2.6 \mu\text{m}$ and $7.4 \mu\text{m}$, for Device and Custom, respectively). In the range of SS less than or equal to 4, all algorithms showed similar and relatively steep slopes, ranging from 7.6 to $10.5 \mu\text{m}$, in the relationship between RNFL thickness and SS, as presented in Table 1.

Figure 1D shows the changes in RNFL thicknesses as a function of the corresponding baseline SS. For lower range SS ($SS < 7$), there was a significant increase in RNFL thickness after HDR imaging (mean thickness change $24.5 \pm 10.0 \mu\text{m}$), and the amount of change decreased as SS increased, while less changes in RNFL thicknesses were found in higher range SS ($SS \geq 7$), with mean thickness change $-0.25 \pm 9.6 \mu\text{m}$.

Experiment 2: Effects of Image Quality Enhancement

In all SD-OCT images with poor signal level, there were notable improvements in terms of retinal layer visibility (Fig. 2). The contrast between adjacent retinal layers or between layers with high and low reflectivity becomes more apparent. Subsequently, areas with poor signal level that lead to segmentation failure were accurately segmented after applying the HDR imaging (Fig. 2). Seven out of nine SD-OCT images with segmentation algorithm failure (77.8%) showed successful segmentation after HDR imaging.

For objective assessment using the image quality metrics, the overall SNR of the processed images was statistically significantly lower than the original SNR, while the overall CNR of the processed images showed statistically significant improvement compared with the original (SNR: 23.3 vs. 20.0 dB, CNR: 2.8 vs. 3.0 dB; $P < 0.0001$, paired t -test) (Table 2). A similar trend was noted when analyzing the change in image quality metrics for

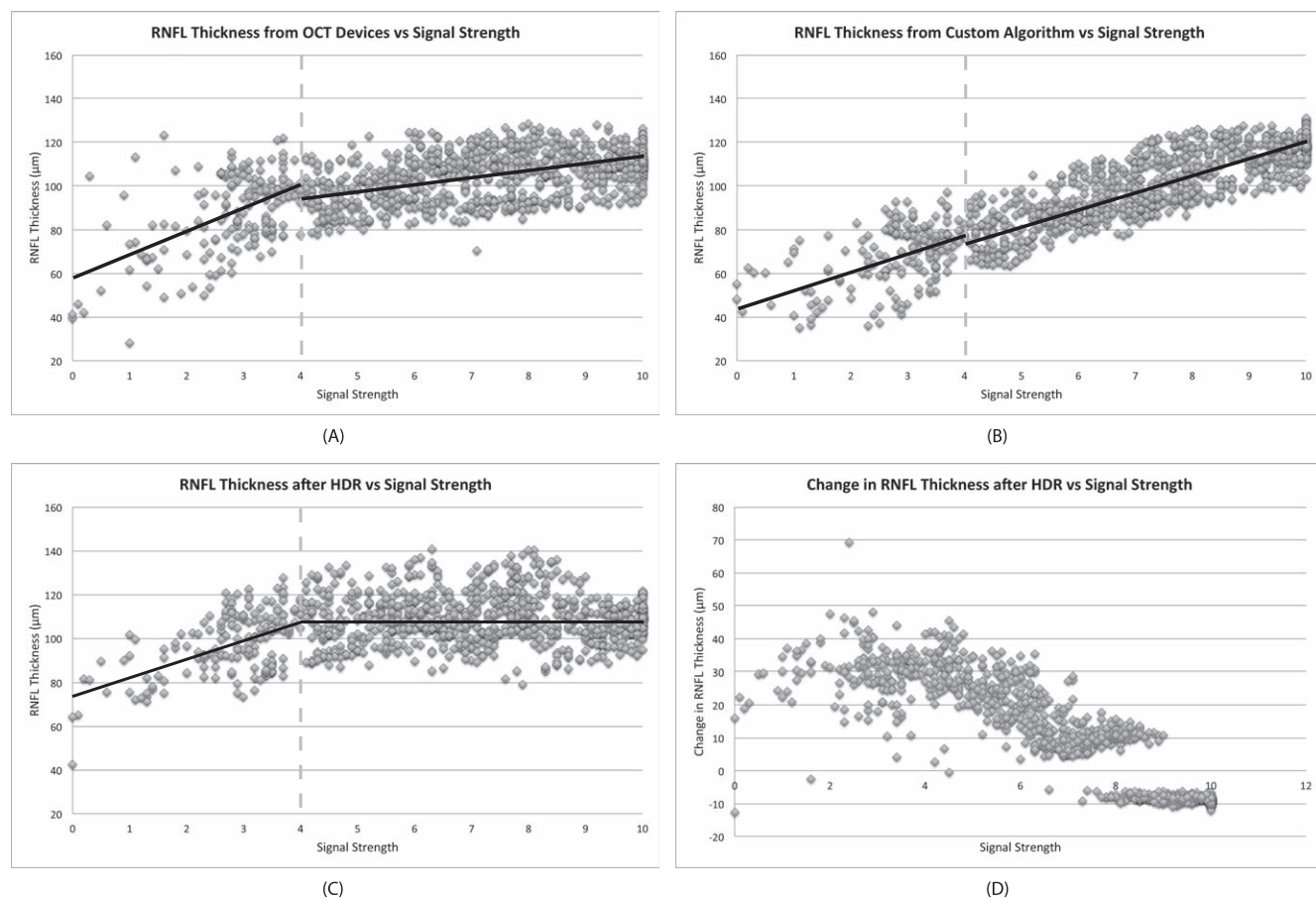


FIGURE 1. Scatterplots of RNFL thickness measurements using (A) the built-in algorithm in TD-OCT devices, (B) our custom segmentation algorithm, and (C) our custom segmentation algorithm after HDR imaging versus SS. The RNFL thickness showed two separate linear relationships with SS less than or equal to 4 and SS greater than 4 for all algorithms. (D) The changes in RNFL thicknesses after HDR imaging as a function of baseline SS.

each imaging device separately. SNR showed a statistically significant decrease for both Cirrus and RTVue data (SNR: 26.2 vs. 20.9 dB for Cirrus, 20.8 vs. 19.1 dB for RTVue, $P < 0.0001$ for both devices, paired *t*-test) while CNR showed statistically significant improvement (CNR: 2.8 vs. 3.1 dB for Cirrus, 2.7 vs. 2.9 dB for RTVue, $P < 0.0001$ for both devices, paired *t*-test).

DISCUSSION

The newly developed HDR imaging technology successfully compensated signal level differences so that RNFL thickness measurement variability across a wide range of SS was minimized to the level of expected measurement variability with good SS. Most retinal layer segmentation algorithms detect the retinal layer boundaries based on the contrast between the adjacent retinal layers. In OCT images with poor

signal quality, the contrast between the adjacent retinal layers was degraded because of low signal level and loss of tissue information. This leads to variable border detection accuracy. The HDR imaging enhanced the image quality in areas with poor signal quality, resulting in the reduction of the RNFL thickness measurement variability.

The algorithm worked well for images with moderately low signal quality ($SS > 4$). For images with extremely low signal quality ($SS \leq 4$), however, the HDR imaging algorithm failed to compensate the low signal quality effect on the RNFL thickness measurement. Clinically, it is a rare case where the best achievable SS is less than 5. In cases of extremely low signal quality, repeated scanning usually results in a scan with higher SS. It is relatively common that the best SS is 5 or 6, especially with older patients with some ocular pathology, which is less than the manufacturer’s recommended acceptable SS of 7. One

TABLE 1. RNFL Thickness Measurements, Slopes, and Intercepts of the Regression Curves of RNFL Thickness Versus SS Using Different Processing Methods

	Signal Strength ≤ 4			Signal Strength > 4		
	Device	Custom	HDR	Device	Custom	HDR
RNFL thickness, μm	86.8 (84.0, 89.7)	68.0 (65.9, 70.2)	97.8 (95.6, 100.0)	104.8 (104.0, 105.5)	100.4 (99.3, 101.5)	109.5 (108.7, 110.3)
Slope, μm	10.5	7.6	9.0	2.6	7.4	-0.01
Intercept, μm	57.8	46.9	72.9	85.4	46.3	109.6

95% confidence interval (CI) of the RNFL thickness measurement is shown in parentheses.

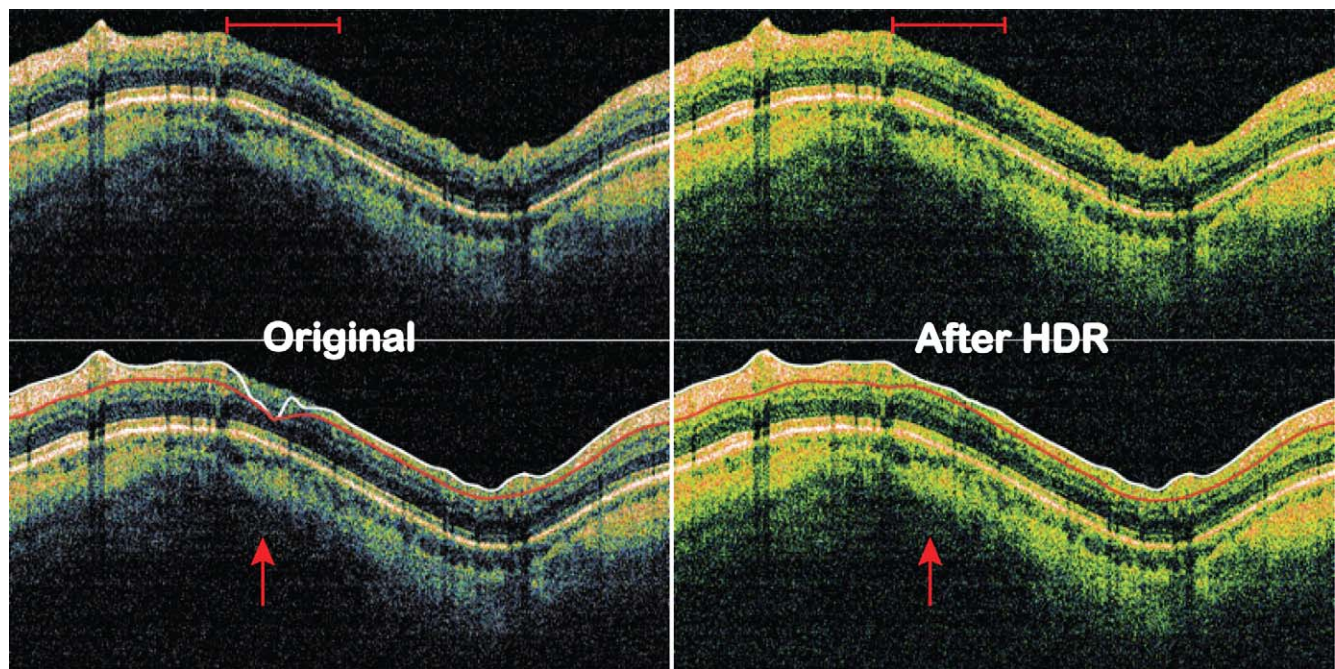


FIGURE 2. SD-OCT images before and after HDR imaging. *Top row:* visibility of the retinal layers became clearer across the image, especially the area within the *red bar* on top. Signal levels also became more homogeneous with HDR imaging. *Bottom row:* RNFL segmentation failed on original image but succeeded after HDR imaging (*red arrow*).

example is a case with one scan with SS equal to 6 and another scan with SS equal to 10 on the same eye showed more than 10 μm difference in RNFL thickness (Device slope $2.6 \mu\text{m} \times 4$ [SS difference]). However, with the HDR imaging, the expected difference is only $-0.04 \mu\text{m}$ (HDR slope $-0.01 \mu\text{m}$), which is negligible. Therefore, images with SS of 5 or 6 may become acceptable for clinical assessment.

HDR imaging also enhanced the visualization of retinal layers and decreased the frequency of segmentation error that is common in poor SS images. The HDR imaging technique divides data from a single OCT image into three virtual channels based on the histogram distribution, mimicking the low, mid, and high exposure images used in the traditional HDR technology in photography. By stretching each channel to the full 8-bit data dynamic range, optimized tissue visualization can be obtained.

Strictly speaking, the presented HDR imaging technique is not a pure HDR technology because three different “virtual exposure” images are created using the same original OCT data, however, the outcome effect is similar in the sense that dynamic ranges of both low and high signal area are expanded.

For objective image quality evaluation, the processed images showed significantly lower SNR, but higher CNR compared with the original images. The decrease of SNR is due to boosting the speckle noise along with the meaningful

signal at very low signal levels. On the other hand, the improvement of CNR agrees with the subjective assessment that HDR imaging enhanced the visibility of fine details of the retinal tissues. Observers tend to look at the signal level on the homogeneous parts of the retina, comparing it against the background, which was the same as how CNR was calculated (Equation 3 and 4), which measures the differences between the signal level of the homogeneous parts of the retina and the noise signal. Both the retinal signal level and the noise signal level were raised after HDR imaging, but the effects on the meaningful signal outperformed the adverse effect on the boosted noise. This indicates that for clinically acceptable high signal level images, our HDR imaging has the ability to improve image quality and enhance the visibility of fine details of the retinal tissues, which may help better clinical diagnoses and image reading.

Even though the noise level increases and SNR decreases after HDR imaging, the HDR imaging fixed some segmentation failures. As with the effects on subjective assessment, similar positive effect was observed on segmentation performance even with the boosted noise. Combined with its compensation effect on RNFL thickness measurement variability, the HDR imaging may provide better RNFL thickness measurement reproducibility and improve accuracy of longitudinal clinical assessment on disease progression. Although in theory the

TABLE 2. Image Quality Assessment Results for Original and HDR Processed Images

	SNR (dB)			CNR (dB)		
	Original	HDR Processed	Diff	Original	HDR Processed	Diff
Cirrus ($N = 124$)	26.20 (26.12, 26.28)	20.94 (20.85, 21.03)	-5.27 (-5.30, -5.24)	2.80 (2.59, 3.01)	3.07 (2.80, 3.34)	0.27 (0.2-0.33)
RTVue ($N = 145$)	20.81 (20.75, 20.88)	19.12 (19.10, 19.17)	-1.69 (-1.72, -1.66)	2.73 (2.64, 2.82)	2.90 (2.81, 2.99)	0.17 (0.16, 0.18)
Overall ($N = 269$)	23.30 (22.97, 23.63)	19.96 (19.84, 20.10)	-3.34 (-3.56, -3.12)	2.76 (2.66, 2.87)	2.98 (2.85, 3.11)	0.21 (0.18, 0.24)

Diff: SNR or CNR difference between the original and the HDR processed. SNR showed statistically significant decrease after HDR imaging ($P < 0.0001$, paired t -test) while CNR showed statistically significant improvement after HDR imaging ($P < 0.0001$, paired t -test). 95% CI for each measurement is shown in the parentheses.

proposed HDR processing can be applied to OCT images regardless of the manufacturer, actual effects need to be tested. Further studies are warranted.

In conclusion, the novel signal enhancement method, which can be applied to both TD- and SD-OCT images regardless of the device, presented herein successfully restored OCT signal and image quality such that RNFL thickness measurement differences between good and poor quality images were reduced to the expected measurement variability.

References

- Drexler W, Fujimoto JG. State-of-the-art retinal optical coherence tomography. *Prog Retin Eye Res.* 2008;27:45-88.
- Huang D, Swanson EA, Lin CP, et al. Optical coherence tomography. *Science.* 1991;22;254:1178-1181.
- Gabriele ML, Wollstein G, Ishikawa H, et al. Optical coherence tomography: history, current status, and laboratory work. *Invest Ophthalmol Vis Sci.* 2011;52:2425-2436.
- Hee MR, Izatt JA, Swanson EA, et al. Optical coherence tomography of the human retina. *Arch Ophthalmol.* 1995;113:325-332.
- Schuman JS, Hee MR, Arya AV, et al. Optical coherence tomography: a new tool for glaucoma diagnosis. *Curr Opin Ophthalmol.* 1995;6:89-95.
- Schuman JS, Hee MR, Puliafito CA, et al. Quantification of nerve fiber layer thickness in normal and glaucomatous eyes using optical coherence tomography. *Arch Ophthalmol.* 1995;113:586-596.
- Schuman JS, Pedut-Kloizman T, Hertzmark E, et al. Reproducibility of nerve fiber layer thickness measurements using optical coherence tomography. *Ophthalmology.* 1996;103:1889-1898.
- Stein DM, Wollstein G, Ishikawa H, Hertzmark E, Noecker RJ, Schuman JS. Effect of corneal drying on optical coherence tomography. *Ophthalmology.* 2006;113:985-991.
- Sung KR, Wollstein G, Schuman JS, et al. Scan quality effect on glaucoma discrimination by glaucoma imaging devices. *Br J Ophthalmol.* 2009;93:1580-1584. Epub 2009 Aug 18.
- Barkana Y, Burgansky-Eliash Z, Gerber Y, et al. Inter-device variability of the Stratus optical coherence tomography. *Am J Ophthalmol.* 2009;147:260-266.
- Stein DM, Ishikawa H, Hariprasad R, et al. A new quality assessment parameter for optical coherence tomography. *Br J Ophthalmol.* 2006;90:186-190.
- Huang Y, Gangaputra S, Lee KE, et al. Signal quality assessment of retinal optical coherence tomography images. *Invest Ophthalmol Vis Sci.* 2012;53:2133-2141.
- Huang J, Liu X, Wu Z, et al. Image quality affects macular and retinal nerve fiber layer thickness measurements on fourier-domain optical coherence tomography. *Ophthalmic Surg Lasers Imaging.* 2011;42:216-221.
- Adler D, Ko T, Herz P, et al. Optical coherence tomography contrast enhancement using spectroscopic analysis with spectral autocorrelation. *Optics Express.* 2004;12:5487-5501.
- Liu Y, Liang Y, Tong Z, et al. Contrast enhancement of optical coherence tomography images using least squares fitting and histogram matching. *Opt Commun.* 2007;279:23-26.
- Salinas HM, Fernández DC. Comparison of PDE-Based nonlinear diffusion approaches for image enhancement and denoising in optical coherence tomography. *IEEE Transactions on Medical Imaging.* 2007;26:761-771.
- Debevec PE, Malik J. Recovering high dynamic range radiance maps from photographs. *ACM SIGGRAPH 2008 Classes.* Los Angeles, CA: ACM, 2008:1-10.
- Durand F, Dorsey J. Fast bilateral Filtering for the display of high-dynamic-range images. *ACM Transactions on Graphics (TOG).* 2002;213:257-266.
- Reinhard E, Heidrich W, Debevec P, Pattanaik S, Ward G, Myszkowski K. *High Dynamic Range Imaging: Acquisition, Display, and Image-Based Light.* Burlington, MA: Morgan Kaufmann Publisher; 2005.
- Bandoh Y, Qiu G, Okuda M, et al. Recent advances in high dynamic range imaging technology. *IEEE Conf Int Conf Image Processing.* 2010;3125-3128.
- Fei P, Yu Z, Wang X, et al. High dynamic range optical projection tomography (HDR-OPT). *Opt Express.* 2012;20:8824-8836.
- Dedrick E, Lau DA. Kalman-filtering approach to high dynamic range imaging for measurement applications. *IEEE Trans Image Process.* 2012;21:527-536.
- Ishikawa H, Stein DM, Wollstein G, et al. Macular segmentation with optical coherence tomography. *Invest Ophthalmol Vis Sci.* 2005;46:2012-2017.
- Adler DC, Ko TH, Fujimoto JG. Speckle reduction in optical coherence tomography images by use of a spatially adaptive wavelet filter. *Opt Lett.* 2004;29:2878-2880.
- Puvanathan P, Bizheva K. Speckle noise reduction algorithm for optical coherence tomography based on interval type II fuzzy set. *Opt Express.* 2007;15:15747-15758.
- Ozcan A, Bilenca A, Desjardin AE, et al. Speckle reduction in optical coherence tomography images using digital filtering. *J Opt Soc Am A* 2007;24:1901.
- Paunescu LA, Schuman JS, Price LL, et al. Reproducibility of nerve fiber thickness, macular thickness, and optic nerve head measurements using StratusOCT. *Invest Ophthalmol Vis Sci.* 2004;45:1716-1724.